Selective Photoinduced Ligand Exchange in a New Tris-Heteroleptic Ru(II) Complex

Bryan A. Albani, Christopher B. Durr, and Claudia Turro*

Department of Chemistry and Biochemistry, The Ohio State University, Columbus, Ohio 43210

1. X-ray Crystallography

Table S1. Crystallographic data for **1**) $[Ru(biq)(phen)(CH_3CN)_2](PF_6)_2$ and **6**) the isolated intermediate $[Ru(biq)(phen)(CH_3CN)(py)](PF_6)_2$

Compound	1	6
chemical formula	$C_{34}H_{26}F_{12}N_6P_2Ru$	$C_{41.55}H_{38.36}F_{12}N_6OP_2Ru$
formula weight	909.62	1028.75
temp (K)	150(2)	150(2)
space group	Triclinic, P-1	Triclinic, P-1
a (Å)	10.2377(2)	9.9878(3)
b (Å)	11.7776(2)	11.8660(3)
c (Å)	15.0852(2)	18.5529(4)
α (^{o})	98.004(1)	98.583(2)
B (^{o})	99.653(1)	92.110(2)
γ (^{o})	97.468(1)	99.059(1)
V (Å^3)	1753.65(5)	2142.96(10)
Z	2	2
D_{calcd} (Mg/m^3)	1.723	1.594
Crystal Size (mm)	0.38 X 0.23 X 0.15	0.22 X 0.38 X 0.38
Theta range for data collection	1.77 to 27.42^o	1.1 to 27.4
μ,(Mo, Kα) (mm^{-1})	0.639	0.535
F(000)	908	1039
Reflections collected	50939	39398
Unique reflections	7967 [R(int)= 0.028]	9727 [R(int) = 0.034]
Completeness to theta max	99.7%	99.7%
Data/restraints/parameters	7967 / 0 / 498	9727 / 139 / 639
R1[a] (%) (all data)	4.79 (5.68)	5.52 (7.7)
wR2[b](%)(all data)	13.61 (14.65)	15.69 (17.82)
Goodness-of-fit on F^2	1.124	1.138
Largest diff. peak and hole (e Å^{-3})	1.300 and -0.642	2.165 and -0.927

[a]R1 = Σ | |F$_o$|-|F$_c$| | / Σ |F$_o$| x 100

[b]wR2 = $[\Sigma$ w (F$_o$^{2}-F$_c$^{2})^2 / Σ (w |F$_o$|^2)$^2]^{1/2}$ x 100
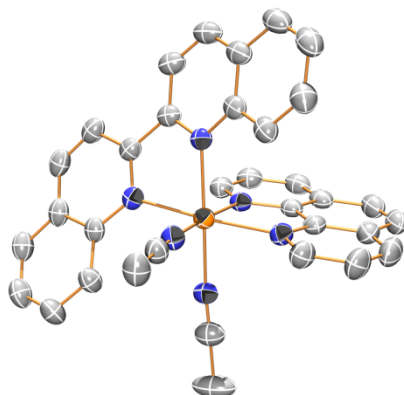
Figure S1. ORTEP plot of complex **1**, [Ru(biq)(phen)(CH₃CN₂](PF₆)₂ (all ellipsoids drawn at 50% probability).
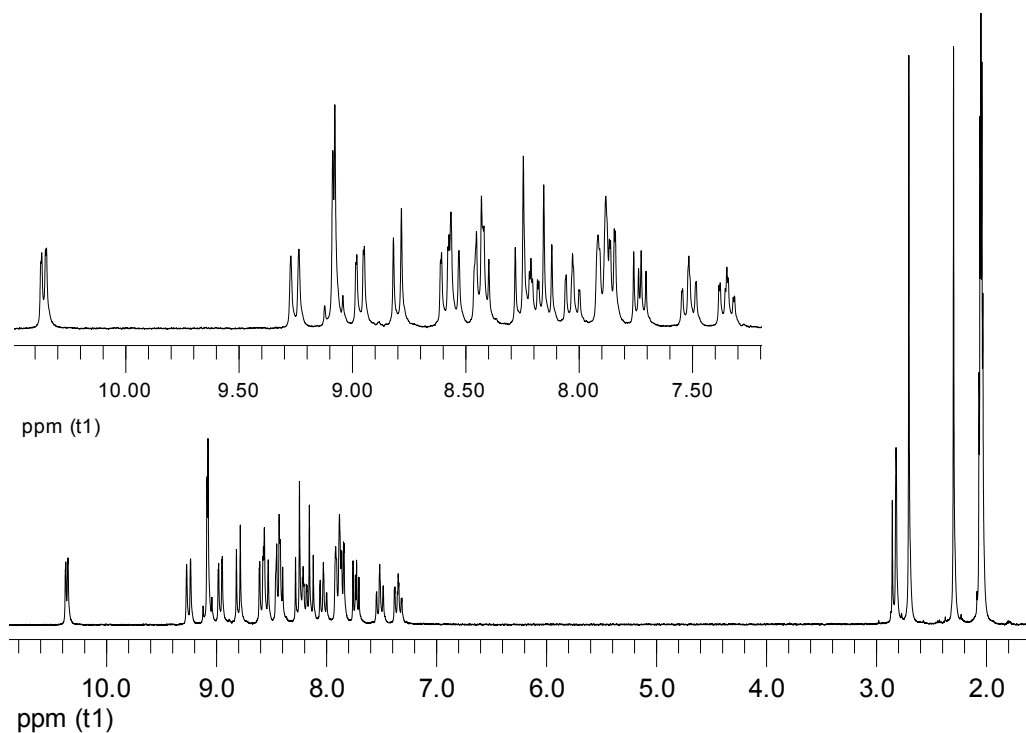

Figure S2. ¹H NMR spectrum of **1** in (CD₃)₂CO. The singlets at 2.3 and 2.7 ppm correspond to the two types of bound acetonitriles. The resonance at ~2.84 ppm corresponds to residual water.
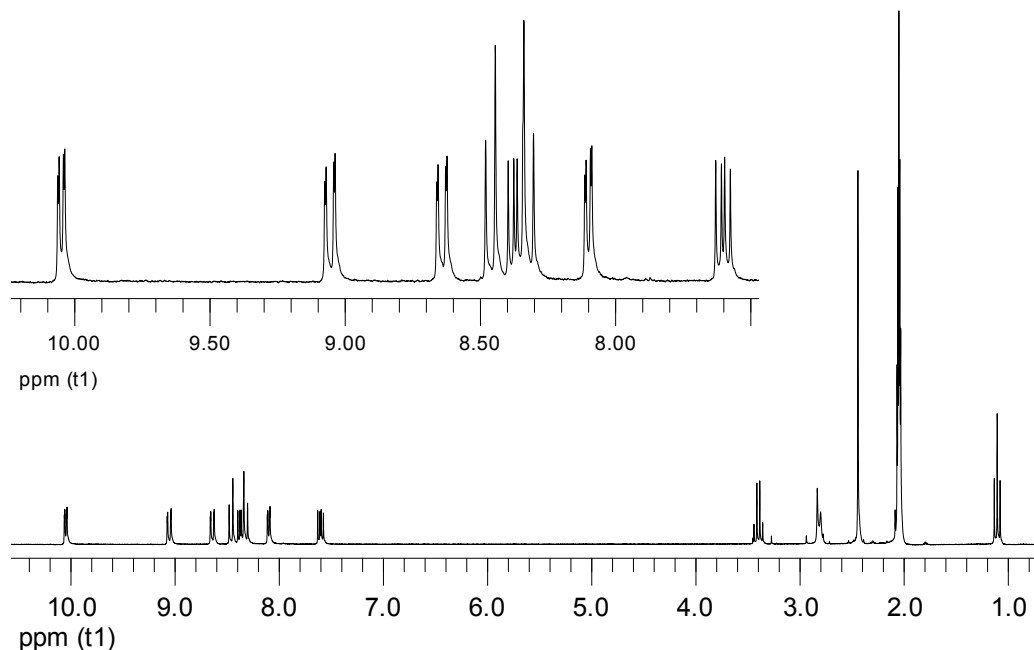
Figure S3. ^{1}H NMR spectrum of **2** in $(CD_3)_2CO$. The resonance at 2.45 ppm integrates to six protons corresponding to both bound acetonitriles. Residual ether solvent peaks appear at 1.1 and 3.4 ppm as well as water at ~2.8 ppm.
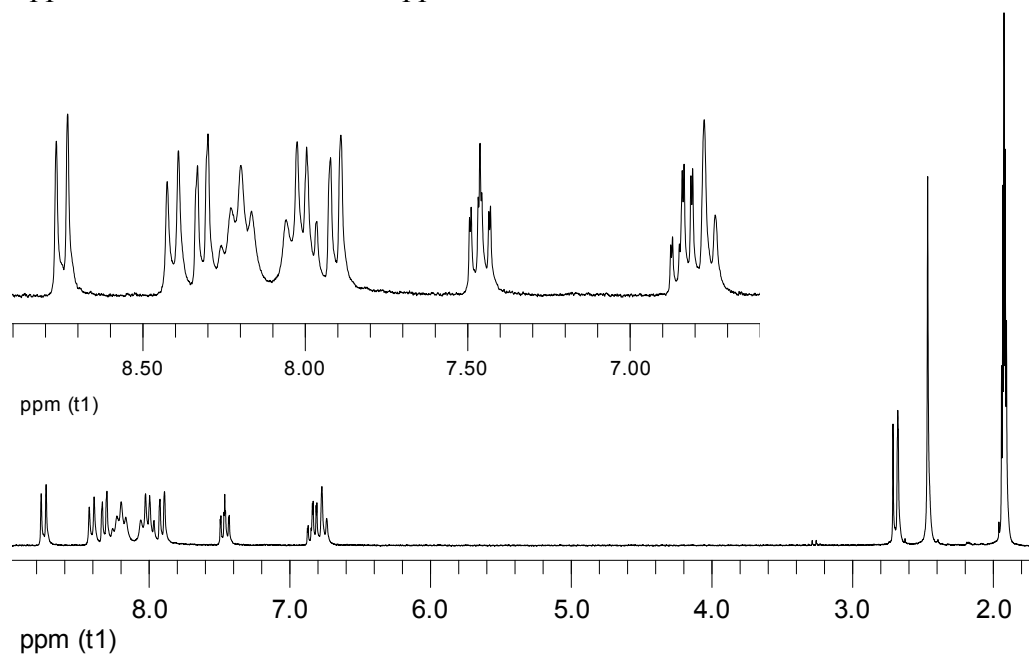

Figure S4. ^{1}H NMR spectrum of **3** in $(CD_3)_2CO$. The resonance at 2.45 ppm integrates to six protons corresponding to both bound acetonitriles.

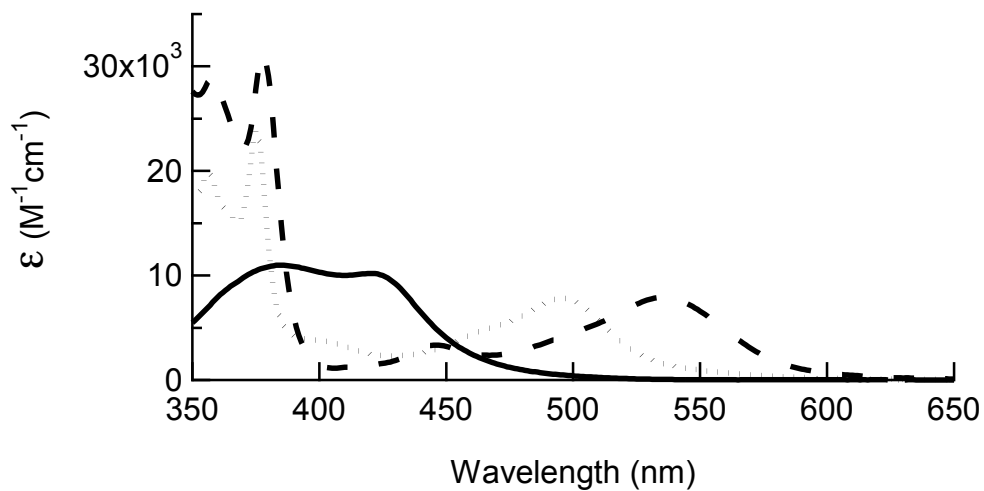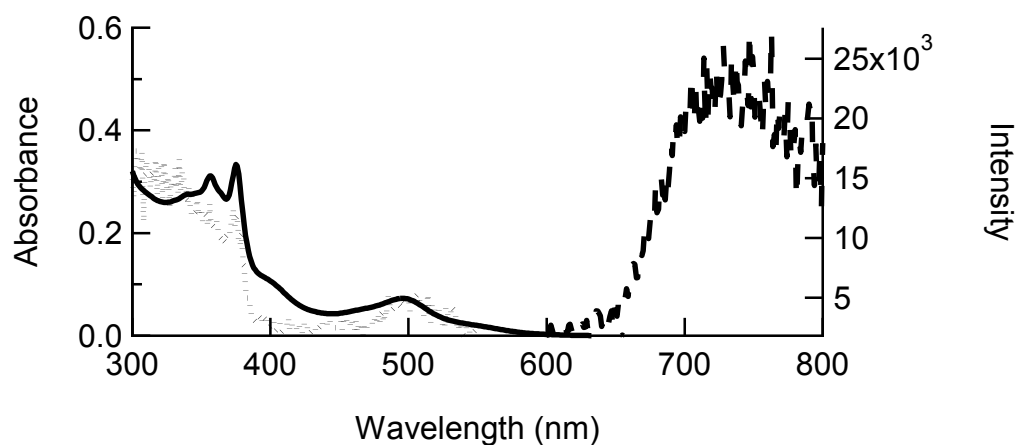**Figure S5.** Electronic absorption spectra in CH$_3$CN of **1** (••••••), **2** (——), and **3** (— —).

Figure S6. Absorption (——), emission (λ_{ex} = 500 nm, — —), and excitation (λ_{em} = 740 nm, •••••) spectra of **1** (10 μM) in CH$_3$CN at room temperature.
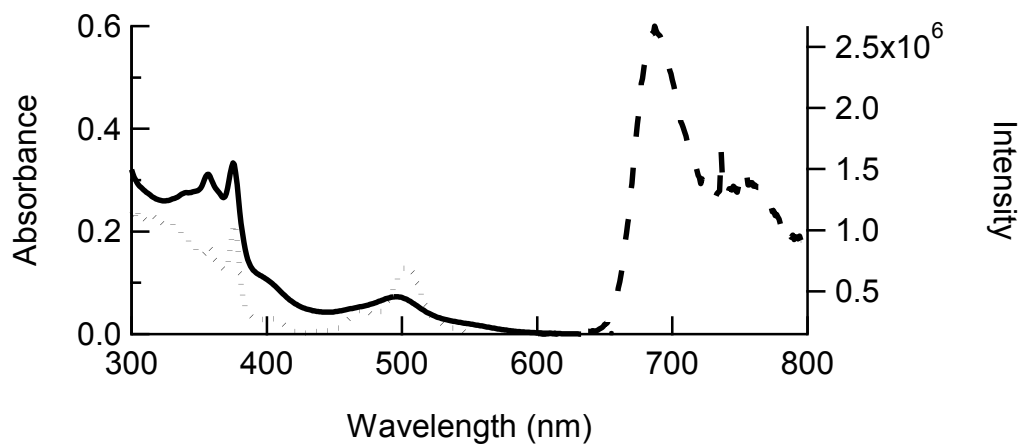
Figure 7. Absorption (▬▬), emission (λ_{ex} = 500 nm, ▬ ▬), and excitation (λ_{em} = 740 nm, ▪▪▪▪▪) spectra of **1** (10 μM) in CH$_3$CN at 77 K.
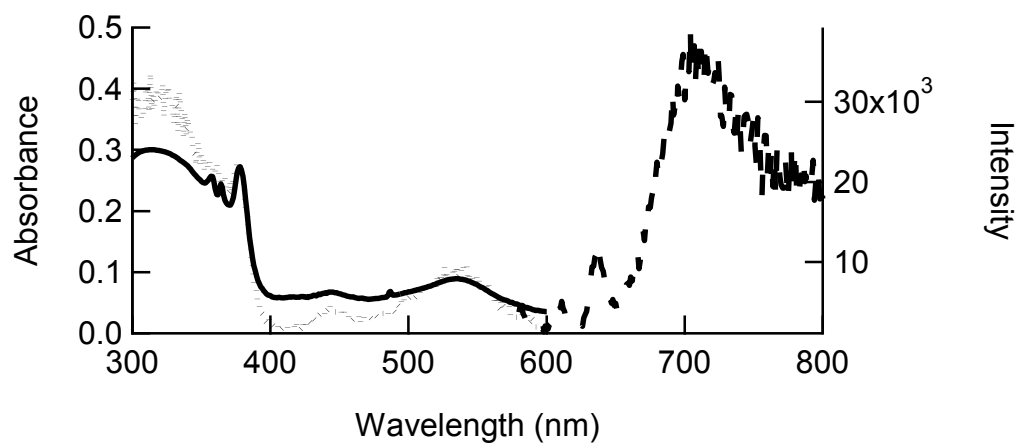

Figure S8. Absorption (▬▬), emission (λ_{ex} = 535 nm, ▬ ▬), and excitation (λ_{em} = 700 nm, ▪▪▪▪▪) spectra of **3** (10 μM) in CH$_3$CN at room temperature.
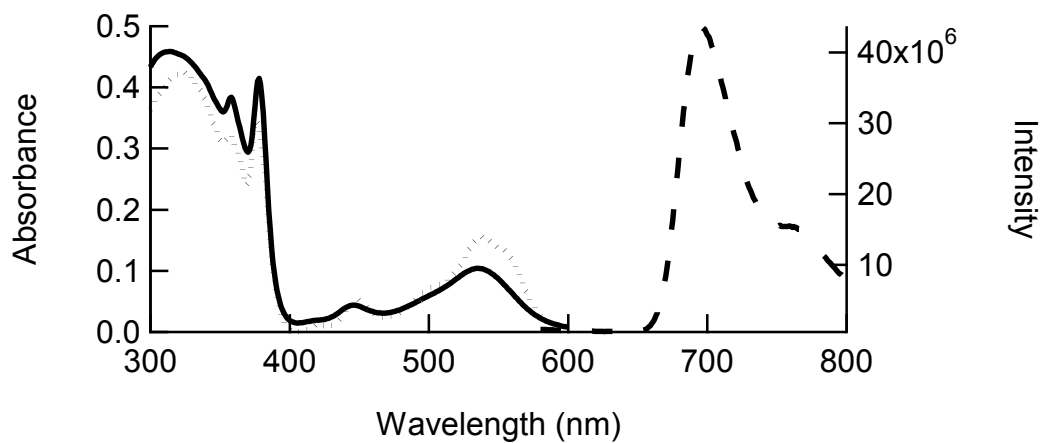
Figure S9. Absorption (———), emission (λ_{ex} = 535 nm, – –), and excitation (λ_{em} = 700 nm, ·····) spectra of **3** (10 μM) in CH$_3$CN at 77 K

Figure S10. Abosrption (———), emission (λ_{ex} = 535 nm, – –), and excitation (λ_{em} = 700 nm, ·····) spectra of **2** (10 μM) in CH$_3$CN at 77 K.
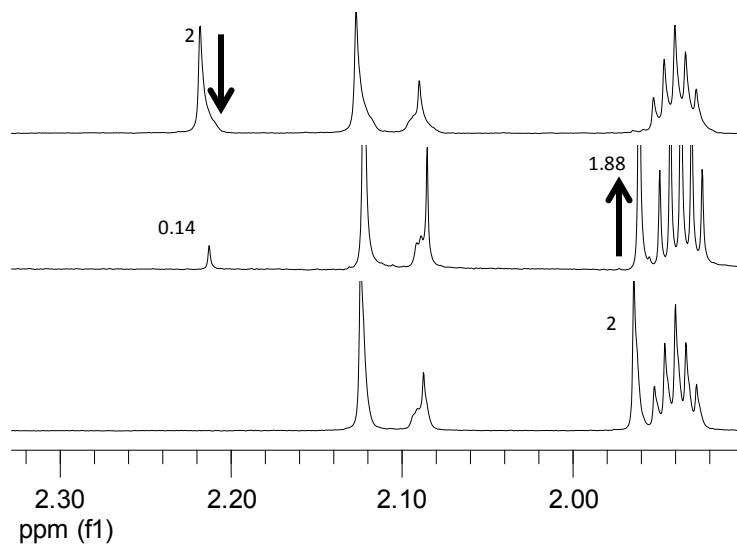
Figure S11. Photolysis of **2** monitored by ^{1}H NMR spectroscopy in CD$_3$CN $\lambda_{irr} \geq 455$ nm at 0, 5, and 20 minutes. Integrations relative to a benzene internal standard are listed next to the corresponding peaks. The resonance at 2.13 ppm and 2.09 correspond to residual water and acetone, respectively, and the singlet growing in at 1.96 ppm corresponds to free CH$_3$CN in solution.
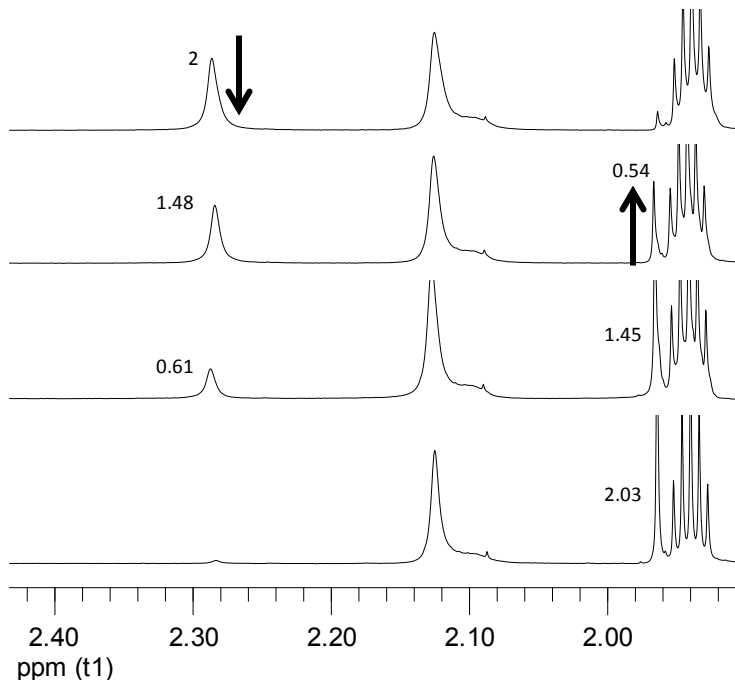

Figure S12. Photolysis of **3** monitored by ^{1}H NMR spectroscopy in CD$_3$CN $\lambda_{irr} \geq 610$ nm at 0, 5, 20, and 60 minutes. Integrations relative to a benzene internal standard are listed next to the corresponding peaks. The resonance at 2.29 ppm corresponds to the bound CH$_3$CN, the
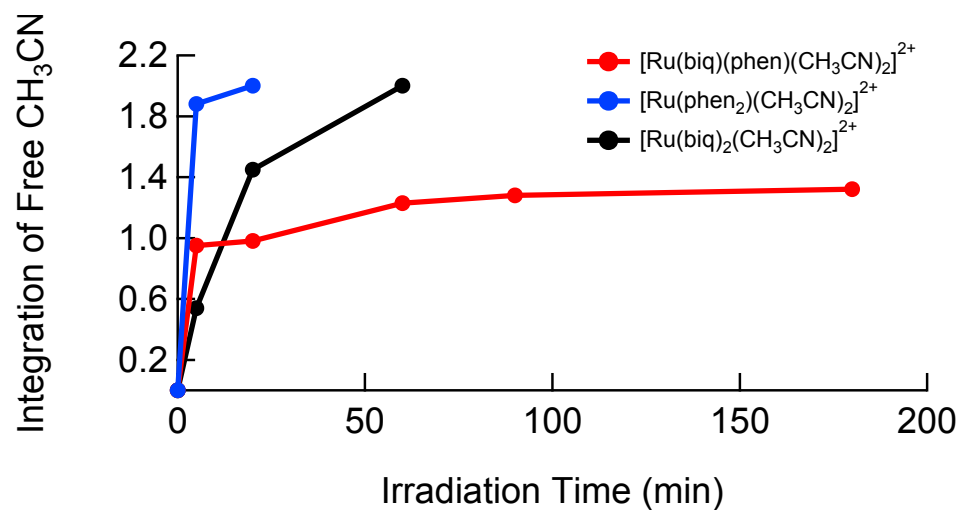
Figure S13. Plot of the integration of free CH_3CN produced vs irradiation time for **1** ($\lambda_{irr} \geq 455$ nm), **2** ($\lambda_{irr} \geq 455$ nm), and **3** ($\lambda_{irr} \geq 610$ nm) in CD_3CN, where the integration corresponding to the three protons of CH_3CN are normalized to 1.0.
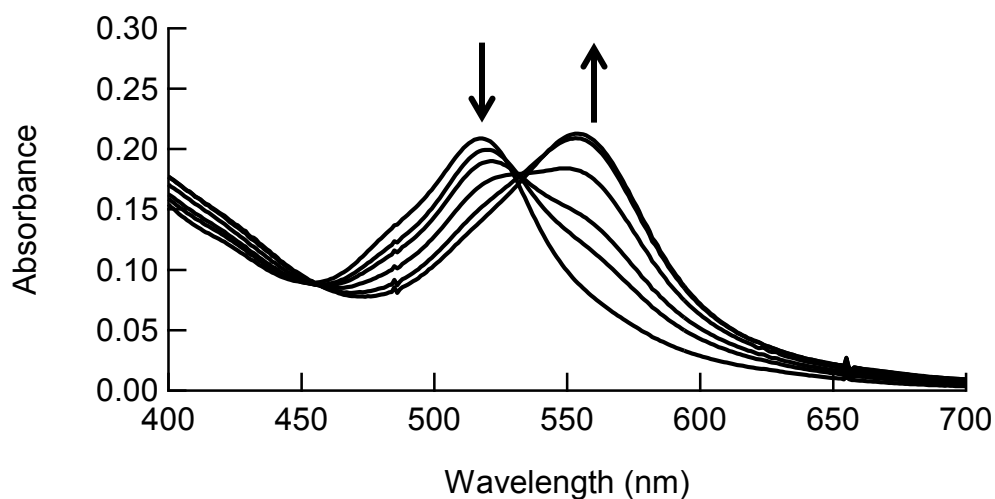

Figure S14. Photolysis of the intermediate $[Ru(biq)(phen)(CH_3CN)(H_2O)]^{2+}$ (**4**) in water over a time period of 3 hours ($\lambda_{irr} \geq 420$ nm).
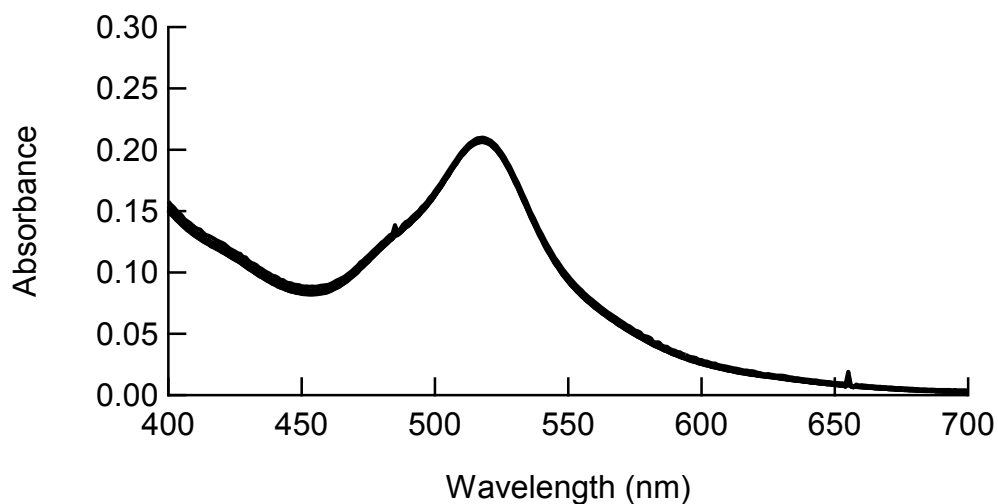
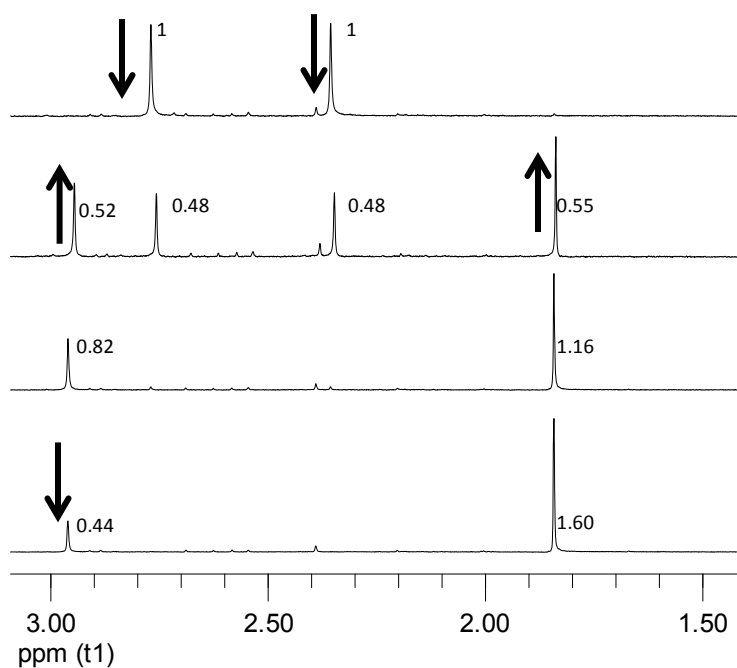**Figure S15.** Thermal Stability of the intermediate [Ru(biq)(phen)(CH₃CN)(H₂O)]$^{2+}$ (**4**) in water over 3 hrous.

Figure S16. Photolysis of **1** monitored by ^{1}H NMR spectroscopy in py - d_5 λ_{irr} ≥ 550 nm at 0, 5, 20, and 60 minutes. Integrations relative to a benzene internal standard are listed next to the corresponding peaks. The initial resonances at 2.35 and 2.75 correspond to bound CH₃CN ligands. The resonances at 2.95 and 1.84 correspond to the bound CH₃CN of the intermediate and free CH₃CN, respectively.

3. Calculations

Table S2. 5 lowest energy singlet excited states obtained from DFT calculations, and the transitions associated with these states in CH_3CN (H = HOMO, L = LUMO) for complex **1'**.

Wavelength (nm)	*f*	Calculated Transitions and Orbital Contributions
476.33	0.0002	H→L(95%), H-3→L(2%)
443.15	0.0646	H-1→L(67%), H-2→L(29%)
429.34	0.0524	H-2→L(65%), H-1→L(27%)
401.57	0.0134	H→L+1(82%), H-1→L+1(7%), H-2→L+1(5%)
390.14	0.0043	H-1→L+1(88%), H→L+1(5%), H-5→L+1(3%)

Table S3. 5 lowest energy singlet excited states obtained from DFT calculations, and the transitions associated with these states in CH_3CN (H = HOMO, L = LUMO) for complex **2'**.

Wavelength (nm)	*f*	Calculated Transitions and Orbital Contributions
395.88	0.0024	H→L+1(81%), H-2→L+1(17%)
395.16	0.0093	H→L(91%), H-2→L(7%)
383.54	0.0054	H-1→L+1(82%), H-2→L(15%)
373.92	0.1128	H-2→L(71%), H-1→L+1(14%), H→L(6%), H→L+3(5%)
369.01	0.0065	H→L+2(43%), H-2→L+1(36%), H-1→L(8%), H→L+1(6%), H-2→L+2(3%)

Table S4. 5 lowest energy singlet excited states obtained from DFT calculations, and the transitions associated with these states in CH_3CN (H = HOMO, L = LUMO) for complex **3'**.

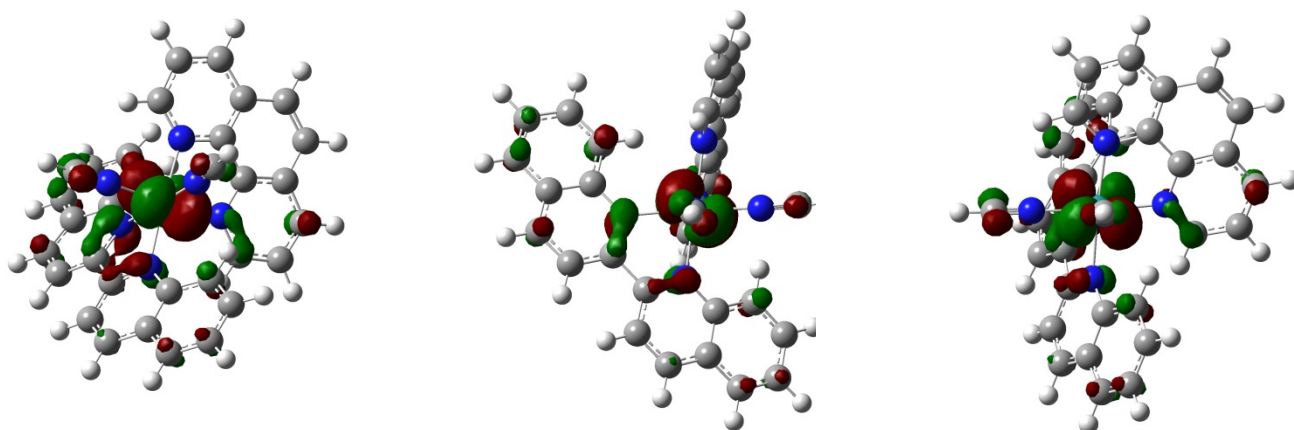| Wavelength (nm)	*f*	Calculated Transitions and Orbital Contributions
495.97	0.0008	H→L(93%), H-1→L(3%), H-7→L(2%)
474.83	0.1015	H-1→L(94%), H→L(2%)
463.45	0.0006	H-2→L(47%), H→L+1(43%), H-3→L(3%), H-5→L(2%)
458.98	0.0006	H→L+1(49%), H-2→L(40%), H-3→L(5%), H-1→L+1(3%)
431.52	0.0007	H-2→L+1(83%), H-3→L+1(11%), H-5→L+1(5%)

Figure S17. Different views of the calculated HOMO in **1'** on geometric optimized structures.
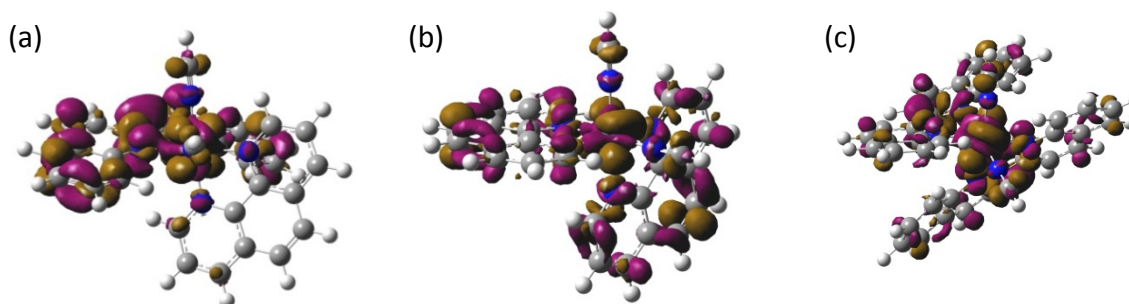

Figure S18. The resulting difference density surface plots of the lowest energy ^{3}MLCT state for (a) **1'**, (b) **2'**, and (c) **3'**. Brown represents removal of electron density and purple represents addition of electron density upon vertical excitation from the minimized singlet ground state.
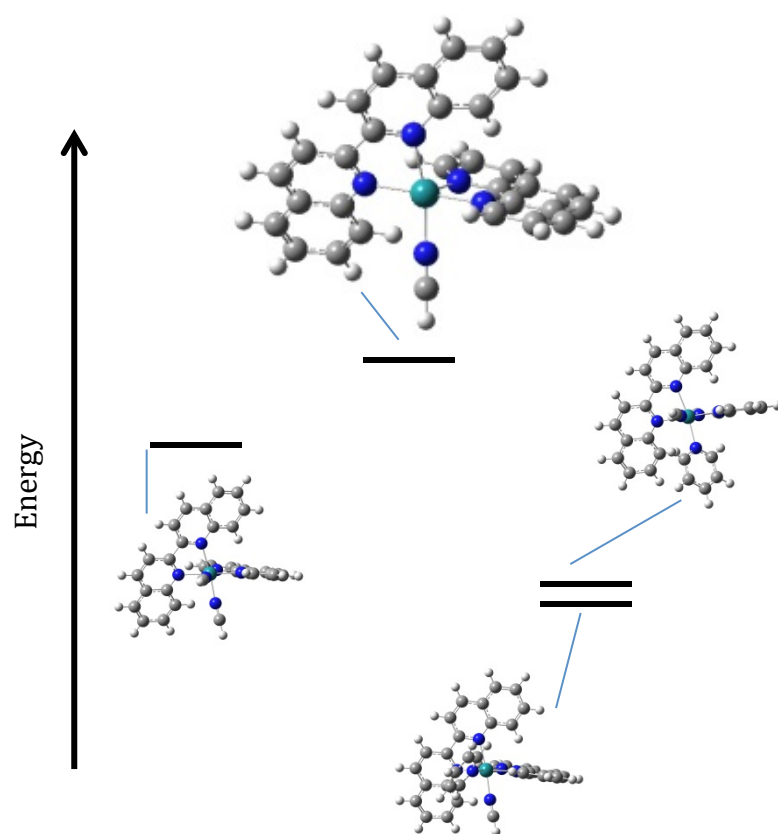
Figure S19. Reaction coordinate representing the possible route to the monosubstituted product upon irradiation in pyridine. The energies of each species are not drawn to scale and the five coordinate intermediate is enlarged for clarity.